Annals of Glaciology 17 1993

Studies of snow surface characteristics by Landsat TM in Dronning Maud Land, Antarctica

JAN-GUNNAR WINTHER
Norwegian Hydrotechnical Laboratory SINTEF NHL, 7034 Trondheim, Norway

ABSTRACT. Large scale melting phenomena like meltwater drainage channels and meltwater accumulation basins or frozen "lakes" have been surveyed on the land ice mass in Dronning Maud Land, Antarctica. These melting features were also detected in a Landsat Thematic Mapper (TM) image recorded on 12 February 1990. Image processing techniques such as principal component (PC) analysis, band ratioing and histogram-equalizing are carried out to emphasize the melting phenomena. Interestingly, a histogram-equalized single TM Band 5 image appears to be a good discriminator, leaving the melting phenomena as bright areas in the TM scene. The largest frozen "lake" is close to 1 km wide while some of the drainage channels stretch more than 5 km. There is also a comparison of satellite-derived and in situ reflectance and temperature. The atmospheric corrected satellite data underestimate surface snow albedo by about 16% while TM measurements of surface temperature are 2° to 6°C lower than that measured on the ground.

INTRODUCTION

Among the wide variety of studies concerning terrestrial phenomena and characteristics, there are advantages in using satellite data for recording, collecting and mapping. Remote sensing enables the processing and interpretation of enormous amounts of data, which is particularly valuable in inaccessible areas like the continent of Antarctica. In addition, the different spectral, temporal, and spatial resolution of satellite sensors make studies of various surface characteristics possible. In this paper, the data acquired from the Landsat-4 TM satellite in February 1990 are used to analyse snow properties and snow conditions in Dronning Maud Land, Antarctica.

Ground-truth measurements were executed during the Norwegian Antarctic Research Expedition (NARE 1989/90) to support the interpretation of the satellite data. Field recordings included measurements of radiation, wind, humidity, heat transfer, air and snow temperature, snow structure, and snow albedo. Weather observations like the amount and type of clouds and observations of surface conditions were also carried out. Hence, a broad in situ data base together with known spectral signatures of snow (Wiscombe and Warren, 1980) supported the following interpretation and analysis of the image. Well-known image processing techniques such as principal component analysis, histogram-equalizing, and band ratioing were applied to the Landsat TM image. At an early stage, large scale meltwater drainage channels and basins of accumulated meltwater (frozen "lakes") were observed within the image. For that reason special interest is taken in finding image enhancement techniques which emphasize these melting phenomena. A histogram-equalized TM Band 5 image is a good discriminator and throws these melting phenomena into relief.

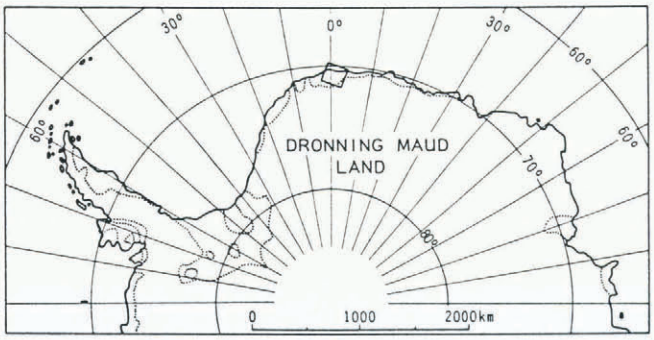

Fig. 1. Index map, showing the location of the image discussed in this paper. The dotted lines show the land boundary of the continent.

Snow melting in Antarctica is limited and occurs occasionally under marginal conditions for melting. Thus, the detected melting phenomena might be sensitive to climate change and be used as climate indicators. A future task should be to analyze how the melting features originate, map their present areal distribution, determine how sensitive they are to climate change, and study changes in the past and possible changes in the future.

THE LANDSAT THEMATIC MAPPER DATA SET

The satellite imagery discussed in this paper is quadrant 4

https://doi.org/10.3189/S026030550001257X Published online by Cambridge University Press

of a Landsat-4 TM scene (Y4276808055X0, path 173 and row 110). The centre of the quadrant is located at 70°55′0″ S and 0°14′0″ E (Fig. 1). The quadrant size is approximately 100 × 85 km. The digital TM data were ordered from Earth Observation Satellite Company (EOSAT) after some pre-examination of black and white photographic products. As a result, the chosen image from 12 February 1990 contains very few clouds. However, severe data saturation occurs in TM Band 1 and this band is excluded in the following analyses. Data saturation is common in regions with high reflection and is reported by many investigators (Dozier, 1985; Orheim and Lucchitta, 1988; Hall and others, 1990a).

Table 1 shows the spectral sensitivity regions for Landsat TM. TM6 lies in the thermal infrared part of the electromagnetic (EM) spectrum and has a spatial resolution of 120 m. All the other bands have a spatial resolution of 28.5 m.

Table 1. Wavelength regions for the Landsat Thematic Mapper Bands (Lillesand and Kiefer, 1987)

Band	*Wavelength region* μm
TM1	0.45–0.52
TM2	0.52–0.60
TM3	0.63–0.69
TM4	0.76–0.90
TM5	1.55–1.75
TM6	10.40–12.50
TM7	2.08–2.35

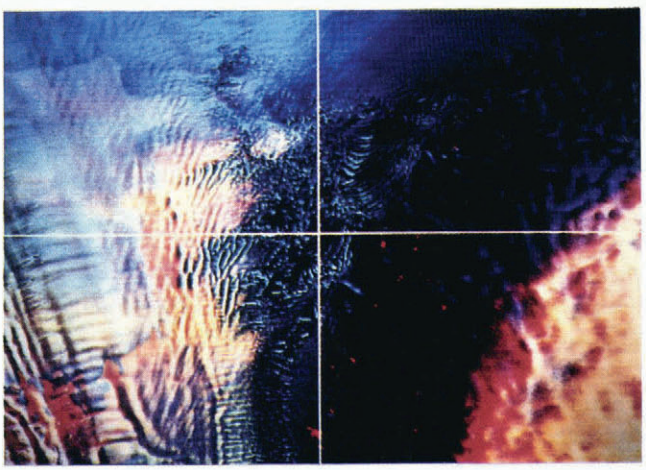

Fig. 2. The figure shows a colour composite image of TM Band 5 (red), TM Band 4 (green) and TM Band 2 (blue). The Jutulstraumen ice stream (lower left quadrant) is flowing out on the sea towards north, forming Fimbulisen (upper left quadrant). The land ice is situated to the right, while the heavily crevassed shear zone, Jutulgryta, appears in the middle of the image. Total image size is 58 km × 58 km, north toward upper left.

Fimbulisen and parts of the land ice mass are situated within the quadrant. Between them lies the heavily crevassed shear zone, Jutulgryta. Figure 2 is a colour composite image of TM Band 5, TM Band 4 and TM Band 2. The displayed area is due north of where the Jutulstraumen ice stream is flowing out on the sea, forming Fimbulisen. Landsat images from this area have been studied and analysed earlier by Orheim and Lucchitta (1987, 1988). We continuously recorded ground-truth parameters on Fimbulisen during the NARE 1989/90 expedition.

SATELLITE-DERIVED REFLECTANCE

After converting the digital numbers (DNs) in the satellite image to surface albedo and surface temperature, a useful comparison can be provided between in situ and satellite-derived measurements. A conversion procedure is described by Markham and Barker (1986). This method is widely used (Hall and others, 1988; Orheim and Lucchitta, 1988; Dozier, 1989) and is applied to the recorded Landsat TM image in this study.

Atmospheric corrections

The satellite sensor observes solar radiation which is backscattered by the Earth–surface–atmosphere system. Thus, the apparent or at-satellite reflectance has to be corrected for the effect of gaseous absorption, scattering by molecules and aerosols, and, to some extent, inhomogeneity in the ground reflectance. A computer code (acronym 5S) is developed to correct for atmospheric effects (Tanré and others, 1990). The input parameters are geometrical conditions (i.e. date and position), atmospheric model (i.e. H_2O, O_3, air pressure and temperature profiles), aerosol model, the spectral band of observation and the ground reflectance (i.e. type and spectral variation). Some of these parameters can be user-defined, or they might be selected from proposed standard conditions (e.g. sub-Arctic winter atmospheric model). For a specified ground reflectance (IGROUND) the corresponding at-satellite reflectance is determined. Then, apparent reflectance might be calculated for different specific ground reflectances, for example with increments of 0.1 (Table 2).

Furthermore, simple linear regression using at-satellite reflectances as the independent variable (X) and ground reflectance as the dependent variable (Y) has been carried out. Once regression equations are established, ground reflectance can easily be calculated for every pixel in the image (Hall and others, 1990b). Table 3 shows the regression equations and corresponding coefficients of determination, R^2.

Comparison with in situ measurements

Satellite-derived surface albedo is calculated for four different surface regimes, Fimbulisen, the shear zone, a frozen "lake", and the rolling north-sloping terrain, respectively (Fig. 2). The corrected narrow-band satel-

https://doi.org/10.3189/S026030550001257X Published online by Cambridge University Press

Table 2. A look-up table showing apparent satellite reflectance for TM Bands 2, 3, 4, 5 and 7, given a specified ground reflectance (IGROUND)

IGROUND	*Apparent (or at-satellite) reflectance*				
	TM2	TM3	TM4	TM5	TM7
0.0	0.035	0.020	0.008	0.001	0.000
0.1	0.111	0.105	0.103	0.096	0.097
0.2	0.188	0.190	0.197	0.191	0.194
0.3	0.266	0.276	0.292	0.286	0.291
0.4	0.346	0.362	0.387	0.381	0.388
0.5	0.426	0.450	0.482	0.476	0.484
0.6	0.508	0.538	0.578	0.572	0.581
0.7	0.591	0.627	0.674	0.667	0.678
0.8	0.675	0.716	0.771	0.762	0.775
0.9	0.761	0.807	0.867	0.858	0.872
1.0	0.848	0.898	0.964	0.953	0.969

Table 3. Simple regression equations expressing the relationship between apparent reflectance (X) and actual (atmospheric corrected) ground reflectance (Y) for TM Bands 2, 3, 4, 5 and 7. The coefficient of determination (R^2) is, as indicated, very high for all TM Bands

Regression equation	R^2
$Y_{TM2} = -0.03176 + 1.230153 \cdot X_{TM2}$	0.9996
$Y_{TM3} = -0.01670 + 1.139264 \cdot X_{TM3}$	0.9999
$Y_{TM4} = -0.00631 + 1.046301 \cdot X_{TM4}$	0.9999
$Y_{TM5} = -0.00057 + 1.050218 \cdot X_{TM5}$	0.9999
$Y_{TM7} = -0.00014 + 1.032378 \cdot X_{TM7}$	0.9999

lite albedos are converted to shortwave albedo (0.4 μm–2.5 μm) to enable comparison with the in situ measurements (Table 4). The incoming solar radiation and surface albedo show a clear spectral dependence (Nikol'skii, 1973; Wiscombe and Warren, 1980). Thus, the contribution from one particular narrow-band (e.g. one TM Band) to the broad-band shortwave albedo varies for different wavelengths. For example, the contribution from the visible part of the EM spectrum is large, since both the solar radiation and the snow albedo display high values at these wavelengths. The integrated albedo does not normally differ much from the albedo derived by the visible TM Bands (Table 4). Consequently, different parts of the EM spectrum have to be weighted according to the combined effect of incoming solar energy and surface albedo. Then, the shortwave or integrated albedo I_a can be estimated as follows:

$$I_a = \sum_{0.4\,\mu m}^{2.5\,\mu m} (SR * A) / \sum_{0.4\,\mu m}^{2.5\,\mu m} SR \qquad (1)$$

where SR is incoming solar radiation at sea level and A is the surface albedo. The integrated albedo, I_a, was computed using Equation (1) for steps of 0.1 μm.

Calculations of solar radiation assume an atmosphere containing 10 mm of water, 0.35 cm of ozone, and aerosol concentration of 200 cm^{-3} at the Earth's surface (Nikol'skii, 1973). Nikol'skii (1973) presents incoming solar radiation for fixed optical air masses, m = 1.0, 1.5, 2.0, 4.0, 6.0 and 8.0. The actual air mass at the time of satellite overpass was calculated by Ashton (1986):

$$m = (\sin \alpha)^{-1} \qquad (2)$$

where α is the solar elevation. Equation 2 gives an optical air mass of 2.5 for α = 23.5°. Then, an interpolation between the curve of m = 2.0 and m = 4.0 was carried out to calculate the spectral incoming solar radiation.

Table 4. Satellite-derived albedo (atmospheric corrected) and temperature for four areas within the Landsat TM image recorded on 12 February 1990. Comparable in situ measurements from Fimbulisen are presented in column 3

Band	*Fimbulisen*		*Frozen "lake"*	*Rough, north-sloping terrain*	*Shear zone*
	n = 14628	In situ	n = 102	n = 10 000	n = 7076
TM2	0.78		0.50	0.72	0.66
TM3	0.75		0.39	0.66	0.60
TM4	0.72 0.72[2]	0.86[1]	0.32	0.60	0.54
TM5	0.07		0.05	0.04	0.04
TM7	0.05		0.04	0.03	0.05
TM6	−25.48°C	−14.2°C	−15.91°C	−17.94°C	−19.82°C

[1] Indicated in situ snow albedo are average albedo values, recorded under clear sky conditions at solar elevations ranging between 10.5° and 35.1°. Consequently, the effects of changing weather conditions on the snow albedo are minimised. The solar elevation during the satellite overpass on 12 February was 23.5°.

[2] Satellite-derived broad-band albedo (0.4 μm–2.5 μm).

https://doi.org/10.3189/S026030550001257X Published online by Cambridge University Press

Finally, the spectral albedo of snow were derived from Wiscombe and Warren (1980).

IMAGE ENHANCEMENT

Principal components

A principal component (PC) analysis is concerned with explaining the variance-covariance structure through a few linear combinations of the original variables. The purpose is both data reduction and improved possibilities for interpretation. The original variables in this case consist of the TM Bands. Then a new set of uncorrelated images are created by a PC-analysis. The first PCs explain most of the variability in the data (Table 5). The calculation of the principal components is based on the correlation matrix and thus removes the effect of within-band variability.

PCs are computed using a 1024 × 1024 sub-image from an area covering parts of Fimbulisen, the shear zone (Jutulgryta) and the land ice mass (Fig. 3). The sub-image is a quarter of the image shown in Figure 2, and located approximately in the middle of the larger image. TM Bands 2-5 and 7 are used in the analysis, creating five PC-vectors each describing the length and direction in a five-dimensional space. PC1 is correlated to all bands, with the largest weight assigned to the visible TM Bands (Table 5). PC2 shows the highest correlation with the infrared TM Bands but highlights pixels with low values in the visible as well. This is particularly pronounced for TM Bands 2 and 3 (Table 5). Overall, this is in agreement with Orheim and Lucchitta (1988) who carried out PC-analysis in the same area.

Table 5. Principal components for a TM sub-image containing Fimbulisen, the shear zone (Jutulgryta), and the land ice mass

	Eigen values	*TM2*	*TM3*	*TM4*	*TM5*	*TM7*	*% of total var.*	*Acc. var.*
PC1	3.58	0.48	0.49	0.51	0.39	0.35	71.58	71.58
PC2	1.10	−0.37	−0.32	−0.20	0.55	0.64	21.96	93.54
PC3	0.23	−0.09	−0.05	0.05	0.72	−0.68	0.69	98.23
PC4	0.07	−0.71	0.11	0.68	−0.14	−0.02	1.43	99.66
PC5	0.02	−0.36	0.80	−0.48	0.04	0.01	0.34	100.00

Contrast stretching

The image display and recording devices normally span a range of 256 grey levels. However, the digital numbers in a satellite image rarely extend over this entire range. In snow-covered areas this is particular pronounced for TM Bands 5 and 7, which have very low reflectance. By using contrast stretching the narrow range of values in the input image is converted to an output image over a wider range of grey levels. When histogram-equalized stretching is applied, output image values are assigned to the display levels on the basis of their frequency of occurrence. Consequently, more display values (and hence more radiometric detail) are assigned to the frequently occurring portion of the histogram (Lillesand and Kiefer, 1987).

The PC1-image is histogram-equalized and filtered by a 3 × 3 low-pass filter (Fig. 3). The pattern to the right reflects the varying surface topography to the land ice. In

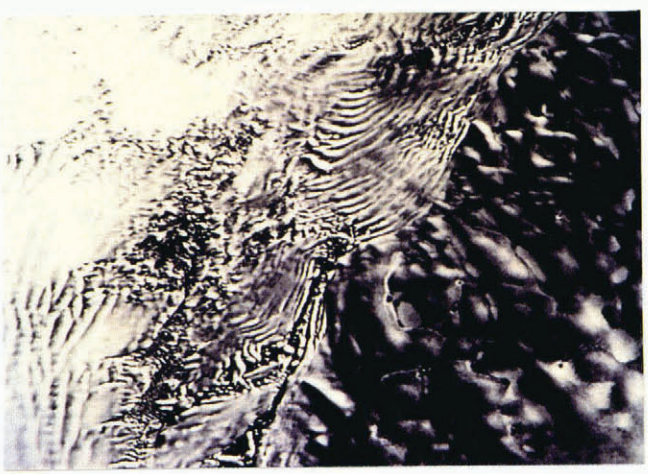

Fig. 3. The PC1-image (29 × 29 km) is a quarter of the image shown in Figure 2 and displays Fimbulisen (left), the heavily crevassed Jutulgryta (middle), and the rolling land ice surface (right). The PC1-image is correlated to the visible TM Bands, and emphasizes topographic features. North is towards the upper left corner, and the solar azimuth is 58.5°.

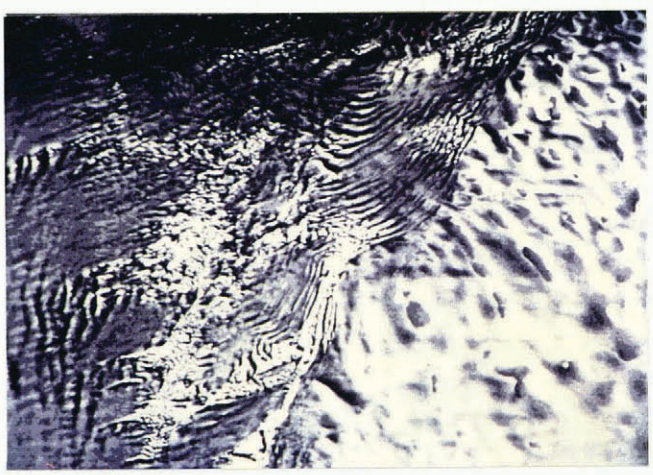

Fig. 4. The PC2-image displays the same area as the PC1-image. PC2 is correlated to the infrared TM Bands and shows the varying properties of the snow surface on Fimbulisen.

https://doi.org/10.3189/S026030550001257X Published online by Cambridge University Press

opposition, the flat surface on Fimbulisen shows small variations in brightness. Between lies the highly rugged and crevassed shear zone giving large reflective variations. Orheim and Lucchitta (1987) concluded that the visible TM Bands are most convenient for studies of topographic features, while TM Bands 5 and 7 are best for the detection of clouds and physical properties of the snow surface. The PC-analysis that was done shows that the PC1-image contains 71.6% of the image variance and is correlated to the visible TM Bands (Table 5). Thus, the PC1-image can be used as a supplement to the visible TM Bands for studies of topographic features.

Figure 4 displays the same area, showing a histogram-equalized and smoothed PC2-image. Overall, the PC2-image contains most details at the smooth surface of Fimbulisen (left part of the image). Since the absolute reflectance in TM bands 5 and 7 is low, PC2 is still correlated with topography. Thus, topographic features like crevasses and the rolling land ice mass (right part of the image) are seen in the PC2-image. However, the brightness variations in PC2 are to a large extent inverted compared to those in the PC1-image. This is especially evident on the land ice mass. Further, a thin and evenly distributed cloud cover is seen above Fimbulisen (Figs 3, 5 and 6). Normally, an even cloud cover like this tends to affect the surface reflectance uniformly. Thus, the distinct spot pattern seen on Fimbulisen is likely to be caused by varying surface characteristics which are enhanced by TM Bands 5 and 7 (Fig. 4). This is not unknown, since an alternating surface spot pattern consisting of loose and edged snow grains and glazed snow with 2–5 mm high ripples perpendicular to the prevailing wind direction was seen close to this area. However, a clear interpretation of PC2 is difficult, since the image also has a considerable correlation to the visible TM Bands (Table 5).

Evidently, the drainage pattern has been brought out clearly in the histogram-equalized TM Band 5 image (Fig. 5, lower right). In theory, one should expect lower TM Band 5 reflectance for ice and highly metamorphosed snow found in the melting areas than for the less metamorphosed surrounding snow. Nevertheless, because of the small albedo differences between ice crystals and snow grains at these wavelengths, even small changes in the apparent ice albedo could cause the bright signal return seen in Figure 5. For example, the high TM Band 5 reflectance could be explained by the presence of ground fog. However, ground fog is likely to have a less distinct coverage than the well-defined pattern displayed in Figure 5. More likely, randomly oriented crystals of ice cause favourable conditions for anisotropic reflection. If so, the satellite-derived TM Band 5 reflectance have increased slightly due to forward-directed scattering from ice crystals in the melting areas. The TM Band 5 image thus represents a suitable tool for extracting the melting features even though the frozen "lake" albedo is calculated to be 0.04, while the surrounding areas have an albedo of 0.03 (Table 4). Obviously, these small absolute albedo differences favour the use of histogram-equalizing. TM Band 5 is generally used for snow/cloud discrimination because both ice and water clouds are appreciably brighter than snow in this band (Dozier, 1985). This is seen in the upper left, where ice clouds appear as white spots (Fig. 5).

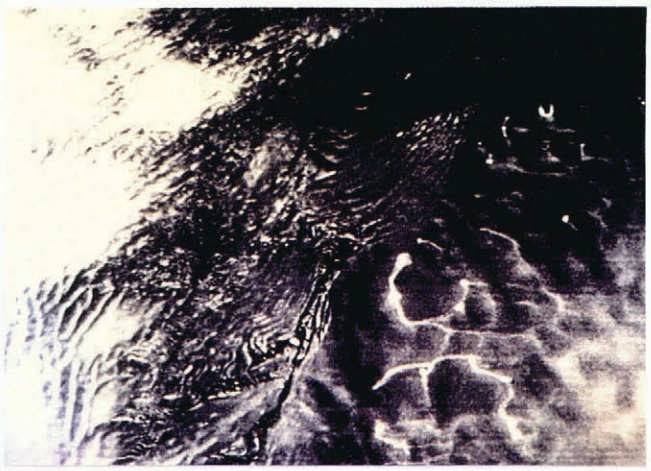

Fig. 5. The single histogram-equalized TM Band 5 image clearly displays the surface drainage channels on the land ice (in the lower right).

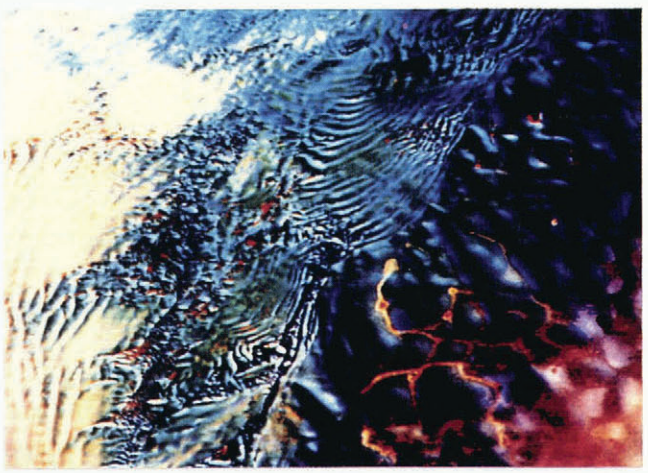

Fig. 6. Colour composite image of TM Band 5 (red), TM Band 4 (green) and TM Band 2 (blue). Note the drainage channels emphasized in the lower right by TM Band 5 (red).

Finally, Figure 6 shows a colour composite image of TM Band 5, TM Band 4, and TM Band 2. TM Band 5 (red) again displays the drainage channels and frozen "lakes" very well.

Band ratioing

Ratioed images display the variations in the slopes of the spectral reflectance curves between two bands, regardless of the absolute reflectance seen in the bands. Consequently, the ratio image has high contrast if the two bands involved show low correlation. Figure 7 shows an image composite of ratio TM Band 2/TM Band 4, ratio TM Band 2/TM Band 5, and ratio TM Band 4/TM Band 5, respectively. These bands were selected since they are located in different regions of the EM spectrum and thus contain complementary information about the character-

https://doi.org/10.3189/S026030550001257X Published online by Cambridge University Press

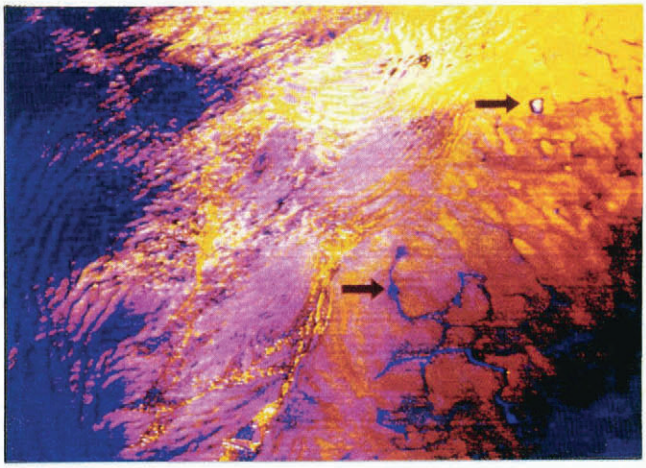

Fig. 7. The image consists of ratio TM Band 2/TM Band 4, ratio TM Band 2/TM Band 5, and ratio TM Band 4/TM Band 5, respectively. Black arrows indicate two frozen "lakes". The upper one was surveyed on 13 February 1990 and is shown in Figure 8.

Fig. 8. The dry meltwater drainage channel surveyed on 13 February 1990 was about 5 m wide. The frozen "lake" consisted of solid ice and its island of snow located in the middle is seen in the background.

istics of the surface. The black arrows show two frozen "lakes". The "lake" in the upper right has a shape like the letter O due to an island of snow located in the middle. This particular area was visited the day after the satellite overpass. Then, the "lake" consisted of pure ice with the exception of some air bubbles and snow crystals which were trapped in the ice body. At that time, the snow melting rate was low, and no water was flowing through the 2–5 m wide meltwater channel draining into the "lake" (Fig. 8). However, it is assumed that meltwater flow takes place during short periods in mid-summer. Then, meltwater flows through the drainage channels but it seems like it freezes rapidly after spreading out on the surface of the frozen "lake". The surface outside the drainage channels consisted of wedges of snow and ice pointing towards the north with an angle corresponding roughly to the solar elevation at noon. The wedges were about 20–40 cm deep, making them effective absorbers of incoming solar radiation.

DISCUSSION AND CONCLUSIONS

Snow melting at such a rate that meltwater flows in the surveyed drainage channels is probably infrequent. Still, this happens occasionally during favourable meteorological conditions. Subsequently, the meltwater collects in depressions and freezes. Large scale melting phenomena such as the drainage channels and basins of accumulated meltwater or "frozen lakes" are also detected using a Landsat TM image taken on 12 February 1990. Processing techniques like principal component analysis, band ratioing and histogram-equalizing are applied to the TM scene to throw these melting features into relief. Interesting, this study indicates that a histogram-equalized single TM Band 5 image is a good discriminator. Obviously, these melting phenomena have a limited areal distribution. Even so, they might be used as climatic indicators. This would require analyses of their formation, past and coming areal variability and sensitivity to climate change.

PC-analysis shows that the first two principal components constitute 93.5% of the total image variance. PC1 is strongest correlated to TM Bands 2, 3 and 4 and is suitable for studies of surface features like topography and crevasses. Topographic effects are seen in PC2 as well. In addition, the PC2-image is highly correlated to TM Band 5 and TM Band 7 which enables studies to be made of snow surface properties. A distinct pattern on Fimbulisen is assumed to be caused by snow drift and snow metamorphosis.

Comparison of satellite-derived and in situ albedo on Fimbulisen shows that the atmospheric corrected satellite data underestimate snow albedo by about 16%. There are several possible explanations for the deviation. First, the standard atmospheric model (sub-arctic winter) used in the 5S computer code may not be convenient for the present meteorological conditions. Improvements might be achieved if the actual atmos-pheric conditions at the time of satellite overpass, i.e. air temperature, air pressure, water vapor, and ozone content at different elevations, were available.

Second, some cirrus clouds were present, especially over Fimbulisen (Fig. 3). Clouds affect the satellite-derived reflectance in the way that the sensed signal not only consists of surface reflectance but also partly of cloud reflectance. The presence of clouds normally increases the measured at-satellite reflectance, especially in TM Band 5 and TM Band 7. Therefore, clouds increase the overall image reflectance and do not explain why the satellite-derived reflectance under-estimate the actual snow albedo. However, the TM Band 5 and TM Band 7 albedo on Fimbulisen is only slightly higher than in the other areas, indicating a moderate influence from clouds (Table 4).

Third, the large difference in sensor resolution is a possible source of error. The Kipp and Zonen CM7 albedometer used for in situ measurements receives most of its radiation from an area within a few square metres, as distinct from the TM-data where each pixel is 28.5 m

https://doi.org/10.3189/S026030550001257X Published online by Cambridge University Press

squared, resulting in a coverage of 812 m^2. Obviously, topographic features larger than the area sensed by the albedometer, will affect the satellite-derived reflectance more seriously than the in situ reflectance. For example, the satellite-derived albedo of the north-sloping and rolling terrain is influenced by shadows due to the low sun angle (Fig. 3).

Then, no attempts have been made to compensate for anisotropic snow reflectance. Freshly fallen snow is nearly a perfect diffuse reflector (Lambertian reflector), while the forward scattering component increases as the snow metamorphoses. Forward scattering tends to increase the off-nadir reflectance relative to the nadir reflectance. Thus, the nadir-viewing Landsat sensors register a slightly lower reflectance compared to the hemispheric reflectance measured by the albedometer (Taylor and Stowe, 1984).

Finally, the in situ albedo is an average albedo recorded under cloud conditions and solar elevations similar to these at the time of satellite overpass. This was necessary, since there is no simultaneous measurement of albedo. Even so, the clear sky albedo varied little and was never below 0.80.

The surface temperature determined on Fimbulisen from TM Band 6 is 12°C lower than the in situ temperature (Table 5). Possible explanations could be: (1) atmospheric conditions and (2) disagreement between the recorded air temperature and surface brightness temperature measured by the satellite. Concerning the latter, it is assumed that the surface can be regarded as a black-body, i.e. the snow emissivity deviates little from unity. Next, the air temperature measured two metres above the surface is supposed to equal the snow surface temperature. The measured snow temperature at the time of the satellite overpass at 5 cm depth was −12.0°C, while the corresponding measured air temper-ature was −13.3°C. Additionally, the in situ data display a temperature gradient in the snow pack with lowest temperature closest to the surface. Thus, there was little deviation between the snow surface temperature and the recorded air temperature.

Disregarding sensor or instrument calibration errors, most of the discrepancy must be attributed to the atmospheric conditions. The 5S code does not correct for atmospheric absorption at TM Band 6 wavelengths. On the other hand, the low temperatures in Antarctica allow only a low water vapor content, resulting in low absorption rates. More important, the presence of clouds would decrease the recorded temperature, as clouds are normally colder than the surface. As mentioned, cirrus clouds were observed from the base camp at Fimbulisen at the time of the satellite overpass. The clouds are seen clearly in the upper left of the TM image (Fig. 5). Unfortunately, the presence of clouds prevents a reasonable comparison with in situ measurements on Fimbulisen.

However, the satellite-derived temperature at the frozen "lakes" and the north-sloping terrain are only slightly lower than the in situ recordings on Fimbulisen (Table 4). Thus, this indicates fairly accurate measurements of temperature. Moreover, these areas are situated 50–150 m higher than the camp on Fimbulisen. An average temperature gradient of 0.7°C/100 m was observed by Orheim and Lucchitta (1988). Assuming such a temperature gradient, the deviations are 1.9°C and 3.5°C, respectively. The shear zone is located at approximately the same elevation as the camp, but satellite-derived temperature there was 6.4°C colder than the in situ temperature. In conclusion, no direct comparable in situ and satellite-derived surface temperatures are available. However, TM Band 6 derived temperature seems to be reasonable but somewhat too low. Finally, Orheim and Lucchitta (1988) calculated satellite-derived temperature in the same region to be 8° to 20°C lower than they measured on the surface. The large temperature deviations were suggested to originate from either sensor or instrument calibration for the temperature range 0° to −20°C.

ACKNOWLEDGEMENTS

The author would like to thank all the participants on the Norwegian Antarctic Research Expedition. A special thanks also to the expedition leader Olav Orheim at the Norwegian Polar Research Institute for valuable support before, during and after the expedition. Jerry Maedel at the University of British Columbia should be acknowledged for his substantial help and guidance during the image processing work. The Norwegian National Committee for Hydrology and the Norwegian Institute of Technology are acknowledged for their funding support. This is publication No. 112 of the Norwegian Antarctic Research Expeditions (1989/90).

REFERENCES

Ashton, G.D., *ed.* 1986. *River and lake ice engineering.* Littleton, CO, Water Resources Publications.

Dozier, J. 1985. Spectral signature of snow in visible and near-infrared wavelengths. *In Proceedings of the 3rd International Colloquium on Spectral Signatures of Objects in Remote Sensing.* Paris, European Space Agency, 437–442. (SP-247.)

Dozier, J. 1989. Spectral signature of alpine snow cover from the Landsat Thematic Mapper. *Remote Sensing Environ.*, **28**, 9–22.

Hall, D.K., A.T.C. Chang and H. Siddalingaiah. 1988. Reflectances of glaciers as calculated using Landsat-5 Thematic Mapper data. *Remote Sensing Environ.*, **25**, 311–321.

Hall, D.K., R.A. Bindschadler, J.L. Foster, A.T.C. Chang and H. Siddalingaiah. 1990a. Comparison of *in situ* and satellite-derived reflectances of Forbindels Glacier, Greenland. *Int. J. Remote Sensing*, **11**(3), 493–504.

Hall, D.K., W.M. Kovalick and A.T.C. Chang. 1990b. Satellite-derived reflectance of snow-covered surfaces in northern Minnesota. *Remote Sensing Environ.*, **33**(2), 87–96.

Lillesand, T.M. and R. Kiefer. 1987. *Remote sensing and image interpretation. Second edition.* New York, John Wiley and Sons.

Markham, B.L. and J.L. Barker. 1986. Landsat MSS and TM post-calibration dynamic ranges, exoatmo-

spheric reflectances and at-satellite temperatures. *EOSAT Technical Notes* 1, 3–8.

Nikol'skii, G.A. 1973. Integrated flux of direct solar radiation. *In* Kondrat'ev, K.Ya., *ed. Radiation characteristics of the atmosphere and the Earth's surface.* New Delhi, Amerind, 289–328.

Orheim, O. and B.K. Lucchitta. 1987. Snow and ice studies by Thematic Mapper and multispectral scanner Landsat images. *Ann. Glaciol.*, **9**, 109–118.

Orheim, O. and B.K. Lucchitta. 1988. Numerical analysis of Landsat Thematic Mapper images of Antarctica: surface temperatures and physical properties. *Ann. Glaciol.*, **11**, 109–120.

Tanré, D. *and six others.* 1990. Description of a computer code to simulate the satellite signal in the solar spectrum: the 5S code. *Int. J. Remote Sensing*, **11**, 659–668.

Taylor, R.V. and L.L. Stowe. 1984. Reflectance characteristics of uniform Earth and cloud surfaces derived from Nimbus-7 ERB. *J. Geophys. Res.*, **93**(C5), 5093–5099.

Wiscombe, W.J. and S.G. Warren. 1980. Solar and infrared radiation calculations for the Antarctic Plateau using a spectrally-detailed snow reflectance model. *In International Radiation Symposium. Volume of extended abstracts.* Fort Collins, CO, Colorado State University, 380–382.

The accuracy of references in the text and in this list is the responsibility of the author, to whom queries should be addressed.